Elastic interfacial waves in discrete and continuous media

E. S. Alber and J. L. Bassani
Department of Mechanical Engineering and Applied Mechanics, University of Pennsylvania, Philadelphia, Pennsylvania 19104

V. Vitek and G. J. Wang
Department of Materials Science and Engineering, University of Pennsylvania, Philadelphia, Pennsylvania 19104
(Received 30 May 1995)

Phonon spectra of bicrystals with relaxed grain-boundary structure display a variety of localized modes including long-wavelength acoustic modes. Continuum solutions for localized waves that incorporate atomic-level elastic properties of the interface via discontinuity relations agree well with the latter modes. In contrast, classical solutions that depend only on bulk elastic properties do not. This demonstrates that the distinct atomic structure of the interface is a controlling factor, and it is shown how local, atomic-level properties can be incorporated into continuum analyses of interfacial phenomena.

I. INTRODUCTION

Distinct grain-boundary structure gives rise to local properties that are significantly different from those in the bulk. In this paper we demonstrate the strong interplay between structure, local elastic properties, and long-wavelength interface waves. For this purpose we have considered crystallographically identical grain boundaries in gold and copper, two fcc metals with nearly identical bulk anisotropy, and find that the localized phonons are strikingly different. For example, the long-wavelength acoustic phonons are highly localized in gold but not at all in copper, while traditional elasticity solutions essentially cannot distinguish the interface waves in these two materials.

Phonons, i.e., elementary harmonic excitations in solids, can reveal important information about structure and properties of interfaces. This has been fully recognized in the case of surfaces[1,2] and a general finding is that surface relaxation/reconstruction must be accounted for to attain agreement between experimental observations and lattice-dynamical calculations.[3] Studies of phonons at internal interfaces, such as grain boundaries, are rather rare,[4] presumably because techniques for direct measurements of phonons at such interfaces are less developed. On the other hand, the propagation of elastic waves along interfaces separating two continua has been analyzed extensively.[5,6] However, in these studies neither the structure nor properties of the interface are taken into account; the interface is simply regarded as a surface across which bulk properties are discontinuous but tractions and displacements are continuous (perfect bonding condition). A significant feature of these solutions is that the condition for the existence of localized interface waves at subsonic velocities (i.e., below the minimum velocity for bulk waves) with the perfect-bonding assumption is rather restrictive.[6–9] These solutions will be referred to as Stoneley waves. Related phonon calculations[10,11] that neglect relaxation at grain boundaries reached similar conclusions, as one would expect.

In this paper we present calculations of phonons for the $\Sigma=5$ (120)/[001] symmetrical tilt boundary (misorientation 36.9°) in both gold and copper. We concentrate on long wavelengths and identify acoustic phonons corresponding to interfacial waves propagating parallel to the interface. For the propagation direction along the tilt axis Stoneley-type solutions exist while for propagation perpendicular to the tilt axis they do not; since gold and copper have very similar bulk anisotropies, the ''perfect bonding'' solutions are nearly the same for each.[9] In contrast, interface phonons are quite different for gold and copper. We show that continuum analyses can reproduce the long-wavelength interfacial phonons only if the elastic properties of the relaxed grain-boundary structure[12] are explicitly included.

II. GRAIN-BOUNDARY STRUCTURES

Calculations presented in this paper have been made for the $\Sigma=5$ (120) symmetrical tilt boundary with the rotation axis [001] corresponding to the misorientation 36.9°. The smallest planar repeat cell of this boundary is delineated by the vectors [001] and [210]. The bicrystal containing this boundary was first constructed geometrically using the coincidence site lattice theory.[13] The atomic structure of this boundary was then determined by minimizing the energy of the bicrystal using a molecular statics method which does not employ periodic boundary conditions in the direction normal to the boundary and simultaneously allows for both the local atomic relaxations and relative rigid-body displacements of the adjoining grains.[14] In these calculations, as well as when constructing the force constants matrix for the phonon studies, we have employed Finnis-Sinclair central force many-body potentials for gold and copper[15,16] which have been fitted to reproduce the lattice parameter, elastic moduli, cohesive energy, and vacancy formation energy. These potentials are analogous to the embedded atom method[17,18] and their functional form was determined on the basis of the second moment of the density of states approximation to the tight-binding method with orbital charge neutrality.[19]

Two alternate structures of this boundary have been found, as in previous pair-potential calculations,[20,21] and these are shown in Figs. 1(a) and 1(b). In the following we denote these structures B and B', respectively. However, unlike in the pair-potential studies where both structures were found to be metastable, the B' structure in gold is unstable

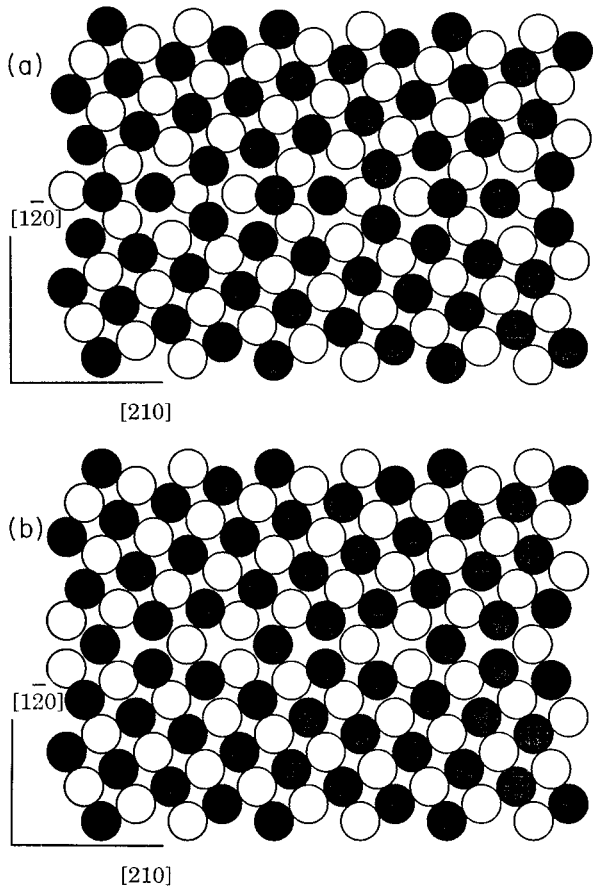

FIG. 1. Atomic structure of the $\Sigma=5$ $(\bar{1}20)/[001]$ projected onto the (001) plane. (a) B structure in gold; (b) B' structure in copper. The white and dark circles represent atoms belonging to two different (002) planes in the [001] period.

and the B structure in copper is unstable. This has been exposed unambiguously in calculations of phonons for the B' structure in gold and B structure in copper which show that some of the phonon frequencies are imaginary.[22,23] This implies that the atomic structures of the $\Sigma=5$ $(120)/[001]$ boundaries are not the same in gold and copper: B is a stable structure in gold and B' in copper.

III. GRAIN-BOUNDARY PHONONS

The phonon calculations have been made using the slab method similar to that commonly employed in surface phonon studies.[3] The repeat cell was defined by vectors $a[210]$, $a[001]$, and $12a[120]$, where a is the lattice parameter, and it contains two boundaries of the above-mentioned type separated by $13.4a$. The atomic positions within the repeat cell were those determined by the molecular statics calculation and no additional relaxation of the three-dimensionally (3D) periodic structure has been carried out. The reciprocal lattice in the (240) plane is body centered tetragonal and has the basis vectors $(1/a)[002]$ and $(2/5a)[210]$. It is shown together with the corresponding Brillouin zone in Fig. 2. Using the usual notation, the calculations were carried out for wave vectors parallel to the vectors $\mathbf{\Gamma X}=(1/5a)[210]$ and $\mathbf{\Gamma Y}=(3/10a)[002]$. In the numerical calculations $\mathbf{\Gamma X}$ and

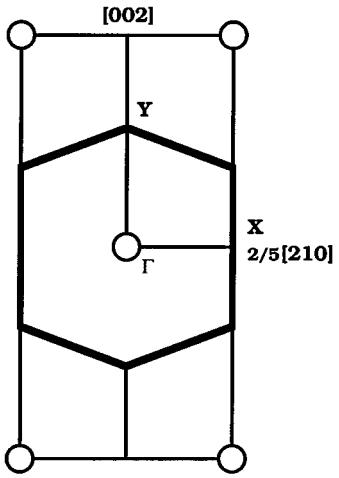

FIG. 2. The reciprocal lattice in the $(\bar{2}40)$ plane and the corresponding Brillouin zone.

$\mathbf{\Gamma Y}$ were divided into twenty steps.

The phonon dispersions calculated for the slab containing the grain boundary in gold (B structure) are shown in Fig. 3(a) and those for the grain boundary in copper (B' structure) in Fig. 4(a). In order to illustrate the connection between bulk and slab dispersion curves, calculations of slab-adapted bulk spectra[24] have also been made in which the same repeat cell as in the case of grain boundaries is used for the ideal fcc lattice. In these spectra, shown in Figs. 3(b) and 4(b), there are 360 modes for each value of $\mathbf{k}$ because the cell contains 120 atoms. Since there are just three acoustic modes for each wave vector in the case of the smallest repeat cell of the ideal fcc lattice, the multiplicity of modes for the bulk crystal corresponds to the well-known folding of the Brillouin zone.[25]

In the case of grain boundaries the lowest frequency modes lie below those of the bulk, i.e., the so-called ''peeling off'' of the lowest frequency modes occurs. New modes with frequencies higher than any of the phonon frequencies in the bulk appear and, finally, vibrational modes fill gaps of the spectrum for the ideal crystal. This is similar to what has been observed in the case of surfaces.[3,26] The low-frequency peeled-off modes are acoustic ($\omega\rightarrow 0$ as $|\mathbf{k}|\rightarrow 0$) while the new high frequency modes are optical and arise because there are nonequivalent atoms in the repeat cell owing to the boundary region. While the phonon spectra are qualitatively similar for gold and copper the ''peel off'' of the acoustic modes is less pronounced and optical phonons much more limited in the case of copper.

Since the goal of this paper is to discuss the link between lattice dynamics and continuum studies of interfacial waves we analyze in detail the long-wavelength acoustic modes. For this purpose Table I summarizes velocities of the long-wavelength acoustic phonons in ideal lattices of gold and copper for the $\mathbf{k}$ vectors parallel to [210] ($\mathbf{\Gamma X}$) and [001] ($\mathbf{\Gamma Y}$) directions, respectively. These velocities, v, were determined on the basis of phonon dispersions shown in Figs. 3(b) and 4(b) using the formula $v=d\omega/d|\mathbf{k}|$. They are in an excellent agreement with the wave velocities calculated using the anisotropic elasticity theory.[9]

In order to investigate the spatial variation of these vibrations we display the real parts of the amplitudes of the lowest-frequency modes for different (240) layers in the re-

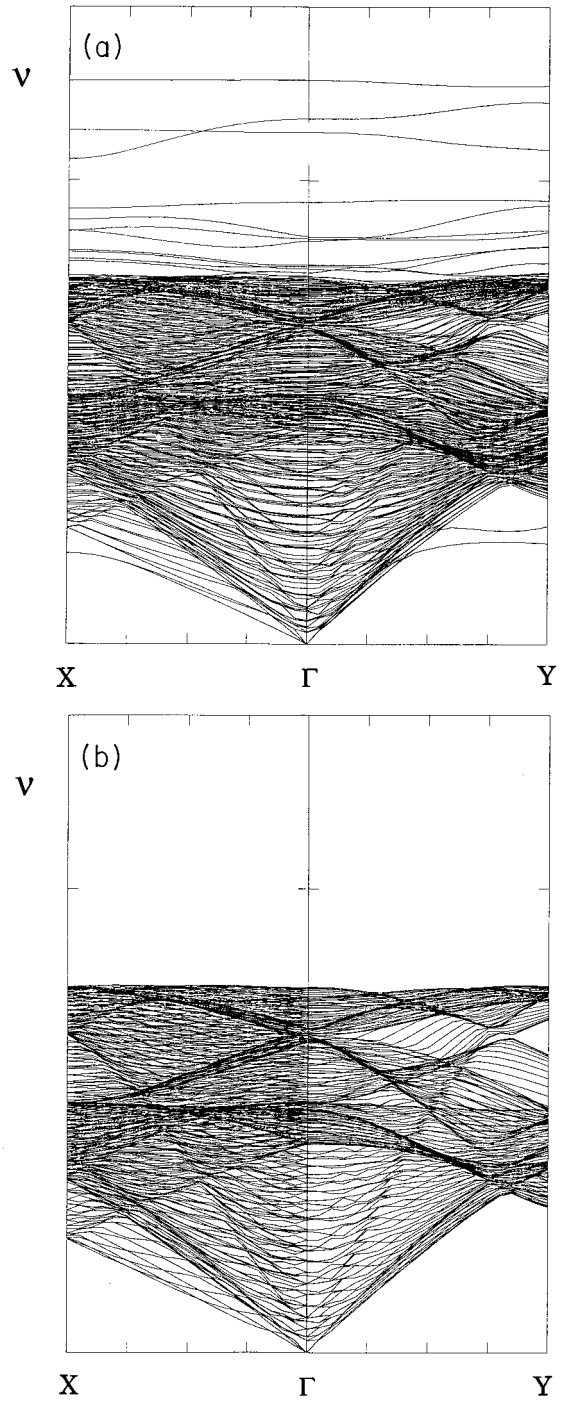

FIG. 3. Phonon dispersions for (a) the bicrystal of gold containing $\Sigma=5$ (120) tilt boundary with the B structure and (b) the perfect lattice of gold.

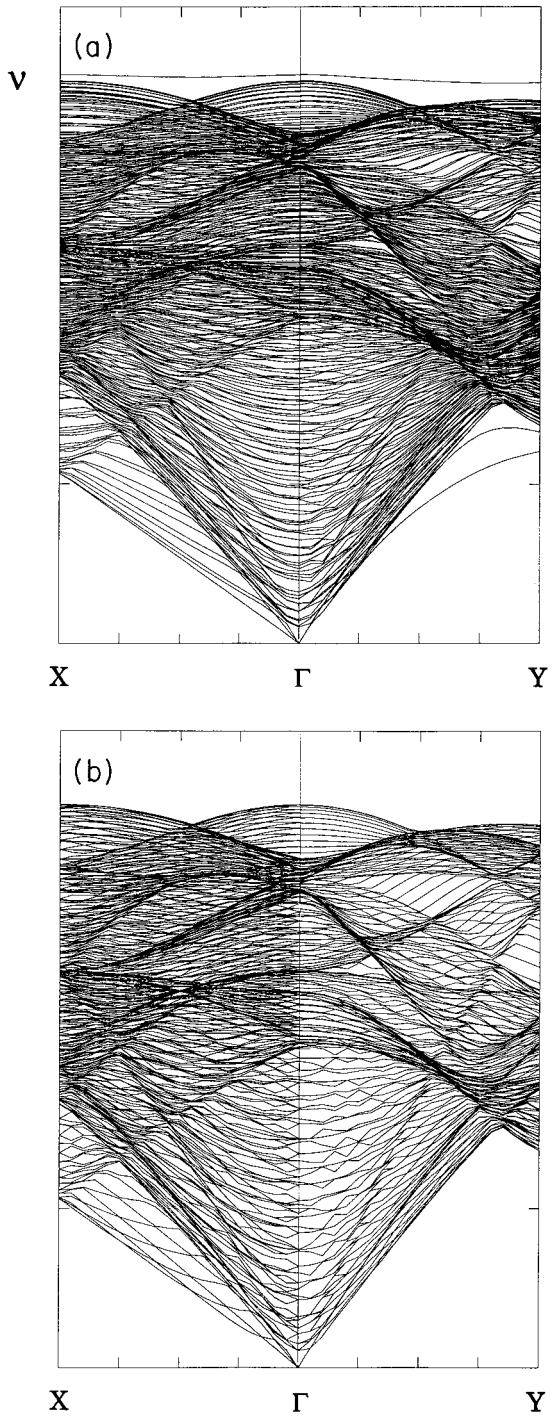

FIG. 4. Phonon dispersions for (a) the bicrystal of copper containing $\Sigma=5$ (120) tilt boundary with the B' structure and (b) the perfect lattice of copper.

peat cell. (The amplitudes are real for $\mathbf{k}=0$ and thus their imaginary parts must be small when $|\mathbf{k}|\rightarrow 0$.) The two grain boundaries present in each repeat cell are positioned in the vicinity of layers 30 and 90, respectively. The real parts of the amplitudes of the first fifteen lowest frequency modes corresponding to $\mathbf{k}=\mathbf{\Gamma Y}/20$ and $\mathbf{k}=\mathbf{\Gamma X}/20$ are shown for the case of gold (B structure) in Figs. 5(a) and 5(b), respectively. The abscissa of these and following plots denotes the number of a particular (240) layer in the repeat cell. The three components of the vibrational amplitudes in the directions [210], [001], and $[\bar{1}20]$ are denoted by the symbols ×, □, and △, respectively (here, and again below, we note that these three directions correspond to x_1, x_2, and x_3, respectively, in the continuum analyses that follow). For three of these modes, 1, 2, and 9 in the case of $\mathbf{\Gamma Y}$ and 1, 2, and 6 for $\mathbf{\Gamma X}$, the dominant directions of vibrations have the largest amplitudes in the boundary region, minimum amplitudes between the boundaries and the amplitudes have the same sign at the two boundaries present in the repeat cell. This indicates localiza-

TABLE I. Velocities (in 10^3 m/sec) of acoustic waves in the bulk calculated from phonon dispersion curves.

Gold	Copper
Wave vector in [210] direction	
1.10	2.07
1.47	2.90
3.25	4.79
Wave vector in [001] direction	
1.47	2.90
1.47	2.90
3.10	4.34

tion of these waves at the boundaries; the reason why their amplitudes are also significant in the bulk is the use of periodic boundary conditions in the direction perpendicular to the boundary. Most of the other modes also display largest vibrational amplitudes in the boundary regions, but in some cases these are of opposite sign at the two boundaries present in the repeat cell (e.g., 3,4,5 in the case of $\mathbf{\Gamma Y}$) or additional maxima (minima) of the same magnitude occur in the region between the boundaries (e.g., 7,8,10–15 in the case of $\mathbf{\Gamma Y}$). This suggests that these are in fact bulklike modes modified by the presence of the boundaries. They correspond to the wave vector $\mathbf{k}=\mathbf{\Gamma Y}/20+n\mathbf{K}_3$, where $-60<n\leqslant 60$ is an integer and $\mathbf{K}_3$ the reciprocal lattice vector in the [120] direction the magnitude of which is $1/|12a[120]|$; i.e., $\mathbf{k}$ is the wave vector from the folded Brillouin zone of the perfect crystal. Modes of this type represent waves propagating in a direction inclined to the boundary plane. They are bulklike and their deviation from the bulk modes in the ideal lattice is merely a consequence of the imposed configuration and periodicity of the repeat cell. In contrast, the modes 1, 2, and 9 in the case of $\mathbf{\Gamma Y}$ and 1, 2, and 6 for $\mathbf{\Gamma X}$ correspond to $n=0$ and represent waves propagating parallel to the boundary plane.

Since in this paper we are interested in waves propagating along the interfaces we always select three lowest frequency modes whose dominant directions of vibrations have the largest amplitudes of the same sign in the boundary regions and minimum amplitudes between the boundaries. These are the modes that will be compared to localized continuum waves. The real parts of the amplitudes for such modes corresponding to $\mathbf{k}=\mathbf{\Gamma Y}/20$ and $\mathbf{k}=\mathbf{\Gamma X}/20$ are shown for the case of gold (B structure) in Figs. 6(a) and 6(b), respectively, and for the case of copper (B' structure) in Figs. 7(a) and 7(b), respectively. The characteristics of these vibrational modes are summarized in Table II.

A common feature of the waves propagating along the $\Sigma=5$ (120) boundary is that for each direction the lowest velocity waves are subsonic, i.e., they propagate slower than the lowest bulk wave (shear) velocity in that direction. This is the case for both gold and copper, but other important features are different in these two materials. First, while the lowest velocity waves are of the same shear type for the $\mathbf{\Gamma X}$ direction, i.e., vertical shear, for the $\mathbf{\Gamma Y}$ direction the lowest velocity wave in gold corresponds to the horizontal shear while in copper to the vertical shear. However, the most pronounced difference is found in the localization of the waves. They are well localized in gold where their amplitudes are largest in the boundary region and decay away from the interface. In contrast, in copper the localization is very weak and the amplitude of the waves is virtually the same for all the atoms in the block. This suggests that the long-wavelength vibrations propagating parallel to the interface depend strongly on the local interface structure. If they did not, these modes would be similar in gold and copper since the cubic anisotropy of the bulk elastic moduli of these two materials is quite similar. Furthermore, the same modes would also exist for the unrelaxed structures and would resemble continuum elasticity solutions of the Stoneley type[5] which decay exponentially away from the interface. These elastic solutions are rather restrictive even in terms of their existence[6] and, as will be discussed below, for the $\Sigma=5$ (120) boundary Stoneley waves can propagate parallel to the tilt axis ([001]) but not perpendicular to the tilt axis ([210]). This is obviously inconsistent with phonon results. This and other incongruities between the phonon calculations and common continuum mechanics solutions are the motive for the development of the mechanical models of interfaces discussed in the following section.

IV. CONTINUUM ANALYSES

The long-wavelength, low-frequency vibrations (phonons) propagating parallel to and rapidly decaying away from the interface depend strongly on the local interface structure, as they do in the case of surface phonons. Below we develop a continuum model that incorporates the local elastic properties of the interfacial region, those that have been calculated for relaxed structures,[12,27] and thereby resolves discrepancies between the calculated phonons and traditional continuum elasticity solutions that neglect interface properties. The continuum solutions are for joined half-spaces, whereas the phonon calculations are for superlattices where each layer (crystal) has a finite thickness. Nevertheless, when the waves are localized in the region of the grain boundaries, as they are for the results shown in Figs. 6 and 7, one anticipates for wavelengths sufficiently less than the boundary spacing that the main features of such waves in that region are not affected significantly by the neighboring boundaries. This is found in the case of the calculated phonons. For a symmetrical bicrystal superlattice, with equal thickness of each layer, formed by tilt about a cube axis, this is precisely the case for the continuum solutions. The proof will be given in a subsequent paper.

Imagine an inhomogeneous interfacial layer of average thickness $2h$ separating two perfect crystals. A simple idealization of this inhomogeneity is obtained by relating jumps in field quantities across the surface between two bulk materials which involve interface constitutive properties. For example, a springlike idealization takes the tractions on the interface to be continuous, as in the case of perfect bonding, but displacement jumps are permitted.[28] If those jumps are linearly related to tractions, with [ ] denoting a jump in field quantity across an interface with normal $\mathbf{n}$, then

$$[\boldsymbol{\sigma}\cdot\mathbf{n}]=0, \tag{1a}$$

$$[\mathbf{u}]=2h\hat{\mathbf{M}}^I\cdot\boldsymbol{\sigma}\cdot\mathbf{n}. \tag{1b}$$

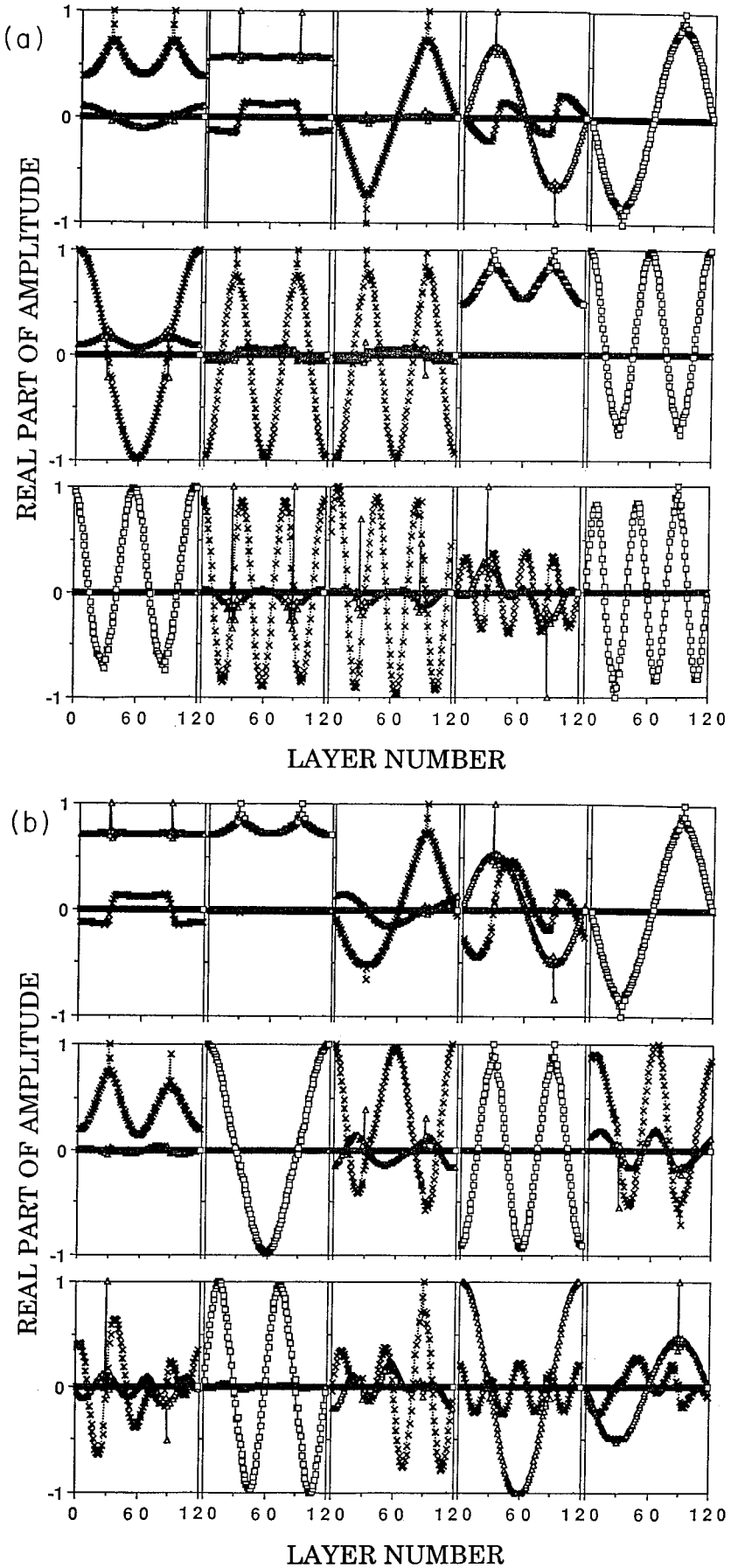

FIG. 5. The amplitudes of the first fifteen lowest frequency modes for the case of gold (*B* structure) corresponding to (a) $\mathbf{k}=\mathbf{\Gamma Y}/20$ and (b) $\mathbf{k}=\mathbf{\Gamma X}/20$.

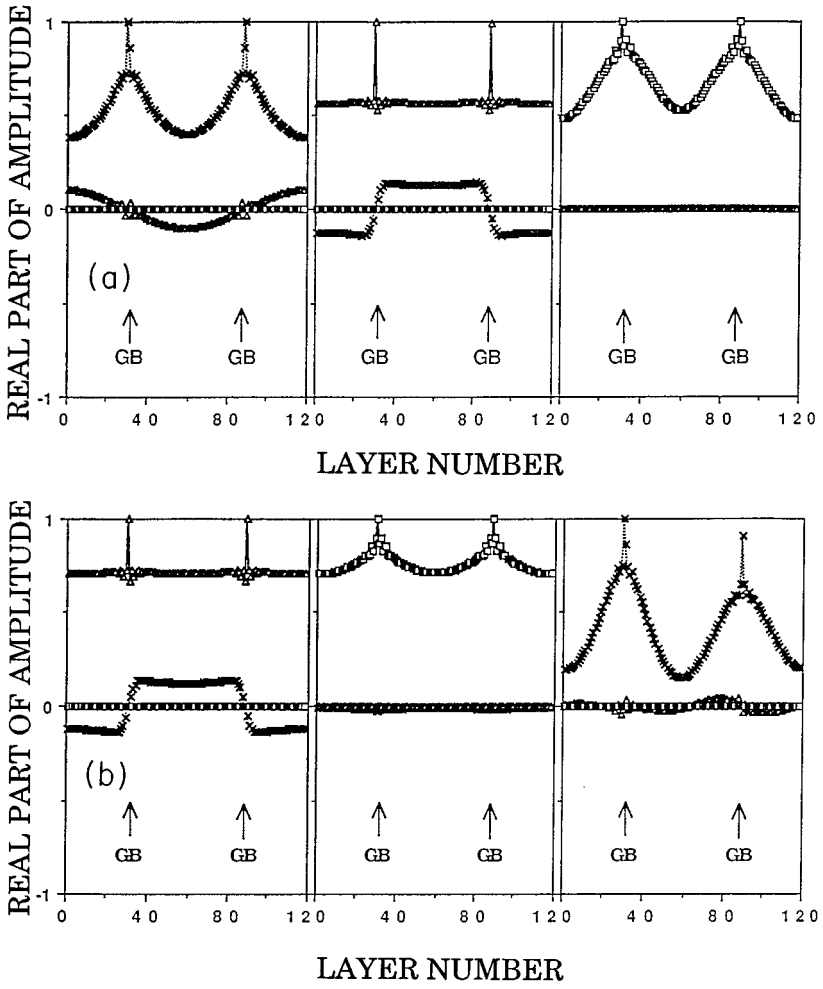

FIG. 6. The amplitudes of three low-frequency interfacial modes for the *B* structure in gold and the wave vectors parallel to (a) **ΓY** ([001]) and (b) **ΓX** ([210]).

An expression for the interface compliance matrix $\hat{\mathbf{M}}^{\mathrm{I}}_{\mathrm{ih}}$ is derived below in terms of the effective properties of the layer that can be computed for the discrete, atomic system.[12] The caret is used to distinguish this second-order tensor (or 3×3 matrix) from the fourth-order tensors of elastic compliance denoted **M** below. (Many examples of spring models describing interfacial behavior can be found in the literature.[28–30])

Consider a 3D inhomogeneous elastic layer of thickness $2h$, in particular one with properties varying in the direction normal to the layer (x_3), subject to traction boundary conditions $T_i=\overline{\sigma_{3i}}$ on $x_3=\pm h$ and $\overline{\sigma_{\alpha\beta}}=0$, $\alpha,\beta=1,2$, where overbars denote volume averages. Integrating the stress-strain relation $2\varepsilon_{i3}=u_{i,3}+u_{3,i}=2M_{i3kl}(x_3)\sigma_{kl}$ with respect to x_3, where **M** denotes the fourth-order tensor of elastic compliance, and assuming that the stress in the layer is uniform and equal to the average stress (Reuss approximation), gives

$$\Delta u_i \equiv u_i\big|_{-h}^{h} = (2-\delta_{i3})\left(\int_{-h}^{h} M_{i3k3}(x_3)\,dx_3\right)\sigma_{k3} \quad (\text{no sum on } i). \tag{2}$$

In this case (or more generally when the stress is only independent of x_3) the direct volume average of Hooke's law $\varepsilon_{i3}=M_{i3kl}(x_3)\sigma_{kl}$ leads to the identification of the integral in (2) with $2hM^{*}_{i3kl}(h)$, where $\mathbf{M}^{*}$ is the tensor of effective compliances that relates the average stress to the average strain in the heterogeneous layer.[31] Then comparing Eqs. (1b) and (2)

$$\hat{M}^{I}_{ik}=(2-\mathbf{e}_i\cdot\mathbf{n})M^{*}_{ijkl}(h)n_jn_l \quad (\text{no sum on } i), \tag{3}$$

where $\mathbf{M}^{*}$ is the tensor of effective interface compliances; its inverse is the effective moduli $\mathbf{C}^{*}$ which, for the results presented below, will be taken from calculations of relaxed grain-boundary structures.[12,27] Note, in general, that $\hat{\mathbf{M}}^{I}$ may not be symmetric, although in the examples considered below it essentially is symmetric.

Next consider two semi-infinite bulk materials with linear elastic moduli (fourth-order tensors) $\mathbf{C}^{(1)}$ for $\mathbf{n}\cdot\mathbf{x}>0$ and $\mathbf{C}^{(2)}$ for $\mathbf{n}\cdot\mathbf{x}<0$ joined by the spring conditions (1) along a planar interface $\mathbf{n}\cdot\mathbf{x}=\mathbf{0}$ where $\mathbf{n}$ is the unit normal to the interface. Interface wave solutions are sought in terms of the displacement fields given in each half-space in the form $\mathbf{u}=\mathbf{a}f(\mathbf{m}\cdot\mathbf{x}+p\mathbf{n}\cdot\mathbf{x}-vt)$ where $\mathbf{m}$ and $\mathbf{n}$ are orthogonal vectors and p and $\mathbf{a}$ are eigenvalues and eigenvectors determined from equilibrium considerations in terms of the Stroh matrices $\mathbf{Q}=\mathbf{m}\cdot\mathbf{C}\cdot\mathbf{m}$, $\mathbf{R}=\mathbf{m}\cdot\mathbf{C}\cdot\mathbf{n}$, and $\mathbf{T}=\mathbf{n}\cdot\mathbf{C}\cdot\mathbf{n}$ and the wave velocity v. Let $\mathbf{P}$ be the diagonal matrix of eigenvalues p and $\mathbf{A}$ be the matrix of corresponding eigenvectors $\mathbf{a}$ associated with equation[6,12]

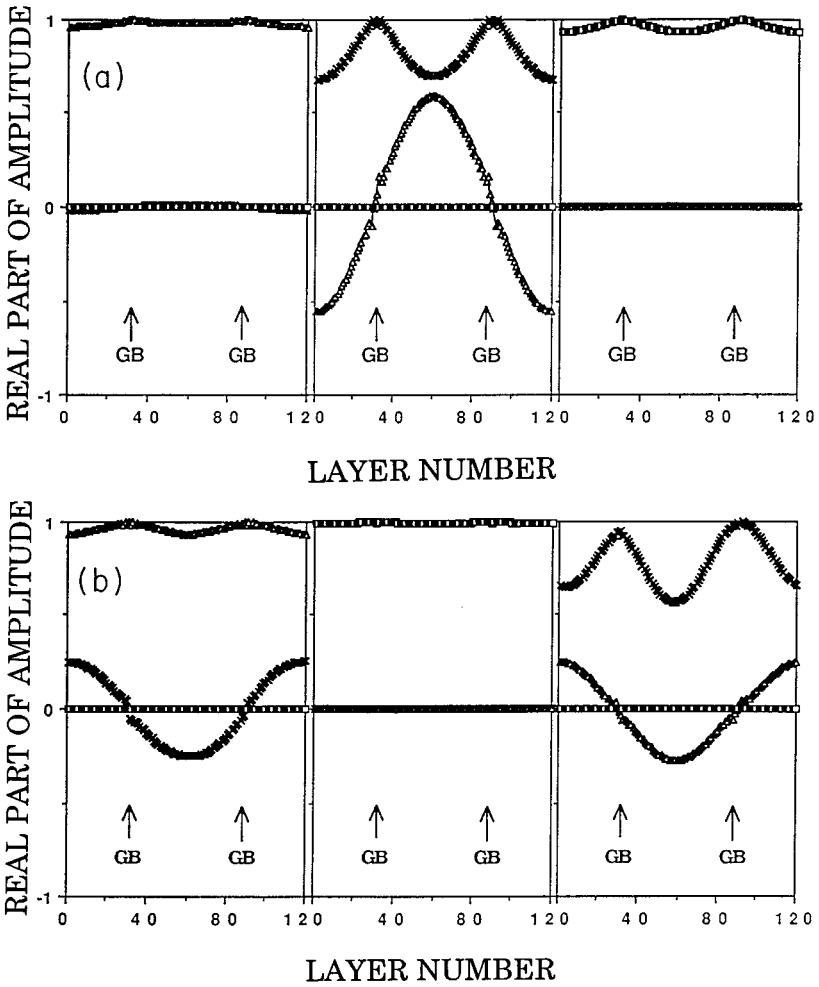

FIG. 7. The amplitudes of three low-frequency interfacial modes for the B' structure in copper and the wave vectors parallel to (a) **ΓY** ([001]) and (b) **ΓX** ([210]).

TABLE II. Acoustic phonon modes localized in the grain boundary for wave vectors parallel to the **ΓX** ([210]) and **ΓY** ([001]) directions. Velocities normalized by the corresponding minimum bulk velocity (from Table I) are given in parentheses.

Gold			Copper		
Dominant direction of vibrations	Character	Velocity (10^3 m/sec)	Dominant direction of vibrations	Character	Velocity (10^3 m/sec)
Wave vector parallel to **ΓX** ([210])			Wave vector parallel to **ΓX** ([210])		
$[\bar{1}20]$	Vertical shear wave	1.06 (0.96)	$[\bar{1}20]$	Vertical shear wave	2.01 (0.97)
[001]	Horizontal shear wave	1.45 (1.32)	[001]	Horizontal shear wave	2.95 (1.43)
[210]	Longitudinal wave	3.25 (2.95)	[210]	Longitudinal wave	4.73 (2.29)
Wave vector parallel to **ΓY** ([001])			Wave vector parallel to **ΓY** ([001])		
[210]	Horizontal shear wave	1.38 (0.94)	$[\bar{1}20]$	Vertical shear wave	2.86 (0.99)
$[\bar{1}20]$	Vertical shear wave	1.54 (1.05)	[210]	Horizontal shear wave	2.94 (1.01)
[001]	Longitudinal wave	3.15 (2.14)	[001]	Longitudinal wave	4.39 (1.51)

$$\{\mathbf{Q}-\rho v^2\mathbf{I}+p(\mathbf{R}+\mathbf{R}^T)+p^2\mathbf{T}\}\cdot\mathbf{a}=\mathbf{0}. \tag{4}$$

The general solutions f are constructed using the interface conditions (1) which introduce the only length scale in the problem, h, and lead to dispersive waves. For harmonic solutions, $f(\xi)=e^{ik\xi}$, waves propagate in the direction of $\mathbf{m}$ and displacements decay exponentially in the direction of $\mathbf{n}$ if $\mathrm{Re}(p^{(i)})=0$, $\mathrm{Im}(p^{(1)})>0$, and $\mathrm{Im}(p^{(2)})<0$. The corresponding displacement and traction fields in the two half-spaces are for $\mathbf{n}\cdot\mathbf{x}>0$

$$u_i^{(1)}=\mathrm{Re}\left\{\sum_{s=1}^{3} d_s^{(1)}A_{is}^{(1)}\exp\{ik(\mathbf{m}\cdot\mathbf{x}+p_s^{(1)}\mathbf{n}\cdot\mathbf{x}-vt)\}\right\}, \tag{5a}$$

$$\sigma_{ij}^{(1)}n_j=-\mathrm{Re}\left\{ik\sum_{s=1}^{3} d_s^{(1)}B_{is}^{(1)}\times\exp\{ik(\mathbf{m}\cdot\mathbf{x}+p_s^{(1)}\mathbf{n}\cdot\mathbf{x}-vt)\}\right\} \tag{5b}$$

and for $\mathbf{n}\cdot\mathbf{x}<0$

$$u_i^{(2)}=\mathrm{Re}\left\{\sum_{s=1}^{3} d_s^{(2)}\bar{A}_{is}^{(2)}\exp\{ik(\mathbf{m}\cdot\mathbf{x}+\bar{p}_s^{(2)}\mathbf{n}\cdot\mathbf{x}-vt)\}\right\}, \tag{5c}$$

$$\sigma_{ij}^{(2)}n_j=-\mathrm{Re}\left\{ik\sum_{s=1}^{3} d_s^{(2)}\bar{B}_{is}^{(2)}\times\exp\{ik(\mathbf{m}\cdot\mathbf{x}+\bar{p}_s^{(2)}\mathbf{n}\cdot\mathbf{x}-vt)\}\right\}, \tag{5d}$$

where $\mathbf{B}=\mathbf{R}^T\cdot\mathbf{A}+\mathbf{T}\cdot\mathbf{A}\cdot\mathbf{P}$ and $\mathbf{P}=\mathrm{diag}\{p_1,p_2,p_3\}$.

Substituting solutions (5) with $\mathbf{n}\cdot\mathbf{x}=0$ into (1a) and (1b) one can write the interface conditions, respectively, as

$$\mathrm{Re}\left\{\sum_{s=1}^{3} d_s^{(1)}B_{is}^{(1)}-\sum_{s=1}^{3} d_s^{(2)}\bar{B}_{is}^{(2)}\right\}=0, \tag{6a}$$

$$\mathrm{Re}\left\{\sum_{s=1}^{3} d_s^{(1)}\bar{A}_{is}^{(1)}-\sum_{s=1}^{3} d_s^{(2)}\bar{A}_{is}^{(2)}-2hki\sum_{s=1}^{3}\sum_{r=1}^{3} d_s^{(1)}\hat{M}_{ir}^{I}B_{rs}^{(1)}\right\}=0. \tag{6b}$$

These conditions are equivalent to

$$\begin{pmatrix}\mathbf{I} & -\mathbf{I}\\ \mathbf{A}^{(1)}(\mathbf{B}^{(1)})^{-1}-(2hki)\hat{\mathbf{M}}^I & -\bar{\mathbf{A}}^{(2)}(\bar{\mathbf{B}}^{(2)})^{-1}\end{pmatrix}_{6\times6}\times\begin{Bmatrix}\mathbf{B}^{(1)}\mathbf{d}^{(1)}\\ \bar{\mathbf{B}}^{(2)}\mathbf{d}^{(2)}\end{Bmatrix}_{6\times1}=\begin{Bmatrix}\mathbf{0}\\ \mathbf{0}\end{Bmatrix}_{6\times1}. \tag{7}$$

For nontrivial solutions of (7) to exist

$$\det[i\mathbf{A}^{(1)}(\mathbf{B}^{(1)})^{-1}+(2hk)\hat{\mathbf{M}}^I-i\bar{\mathbf{A}}^{(2)}(\bar{\mathbf{B}}^{(2)})^{-1}]=0. \tag{8}$$

This dispersion relation can be also rewritten in terms of the interface impedance matrix $\mathbf{H}=\mathbf{Z}^{(1)}+\mathbf{Z}^{(2)}$ which is defined from the surface impedance matrices $\mathbf{Z}=i\mathbf{A}(\mathbf{B})^{-1}=i(\mathbf{R}^T+\mathbf{T}\cdot\mathbf{A}\cdot\mathbf{P}\cdot\mathbf{A}^{-1})^{-1}$ for each half-space as[32]

$$\det[\mathbf{H}+2kh\hat{\mathbf{M}}^I]=0. \tag{9}$$

(The stationary-wave limit[30] is recovered for $v\to0$.) Perfect bonding (Stoneley-type) solutions are recovered from (9) for $h\to0$ or $\hat{\mathbf{M}}^I\to\mathbf{0}$ where the very restrictive necessary condition for nontrivial solutions to exist is $\det(\mathbf{H})=0$ and the corresponding interfacial waves are nondispersive, i.e., their velocity of propagation is independent of wave number k.

Recall that the matrix $\mathbf{H}$ in (9) depends on the elastic moduli of both materials as well as the velocity of propagation v, and it is Hermitian in the subsonic range of velocities,[33] $v<v_b$, where v_b is defined as the minimum bulk wave velocity (typically of shear type) in either material in the direction $\mathbf{m}$. The matrix $\hat{\mathbf{M}}^I$ is real and always positive definite (which is guaranteed if $\mathbf{M}^*$ is at least strongly elliptic). When $\hat{\mathbf{M}}^I$ is symmetric the product $\mathbf{H}(\hat{\mathbf{M}}^I)^{-1}$ is also Hermitian, and, therefore in this case, the eigenvalues $(-2kh)$ are real. If $\hat{\mathbf{M}}^I$ is nonsymmetric, then (9) may admit solutions with the imaginary part of k nonzero. The corre-

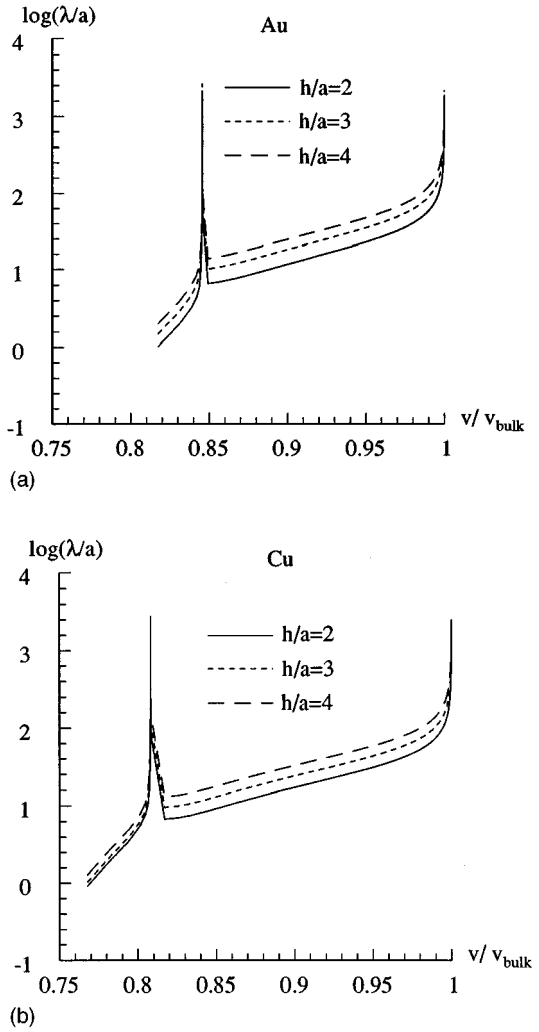

FIG. 8. Wavelength λ (normalized by lattice parameter a) vs velocity v for subsonic interfacial waves propagating along the tilt axis ($\mathbf{\Gamma Y}$) (a) for B structure in gold and (b) for B' structure in copper ($\log=\log_{10}$).

sponding wave is called "leaky," since from (5a),(5c) it does not propagate parallel to the interface and is not strictly harmonic in time. Finally, if the velocity v is regarded as an independent variable we also note that the solutions (5) depend on velocity and bulk properties through $p_s^{(\alpha)}$, $A_{is}^{(\alpha)}$, and $B_{is}^{(\alpha)}$ and additionally on velocity, bulk, and interface properties through k and d_s^{α} which are the eigenvalues and eigenvectors, respectively, associated with (7). If, alternatively, the wave number k is regarded as an independent variable, then the velocity satisfying (9) depends on k as do all the other variables just listed.

These waves will now be investigated for infinite bicrystals with the $\Sigma=5$ (120)/[001] symmetrical tilt grain boundary considered above in gold and copper. For these bicrystals with the effective interfacial compliances obtained from atomistic calculations[12] the off-diagonal elements of $(\hat{\mathbf{M}}^I)^{-1}$ are several orders of magnitude smaller than diagonal elements, so that antisymmetric part of $(\hat{\mathbf{M}}^I)^{-1}$ is indeed small [note for symmetric tilt about the x_2 cube that $\hat{\mathbf{M}}^I$ (3×3) derived from $1/2(\mathbf{M}^{(1)}+\mathbf{M}^{(2)})$ in place of $\mathbf{M}^*$ in (3) is indeed symmetric]. Hence the imaginary part of k_i, $i=1,3$, is also several orders of magnitude smaller than the real part and the corresponding solutions are essentially propagating harmonic waves.[34] For this bicrystal, among the three mathematical branches of solution (k_1, k_2, and k_3) only one is physically realistic in the sense that the real part of k is positive for all velocities in the subsonic range.[35] Also for this bicrystal type, i.e., with a symmetrical tilt grain boundary formed by joining two cubic crystals rotated about a cube axis, one partial interfacial wave is uncoupled. For the $\Sigma=5$ (120)/[001] grain boundary under consideration, the latter partial wave is the only one for which $k>0$ for all $v<(v_{\text{bulk}})_{\min}$.

Since the mode with $\text{Re}\{p\}=0$ propagates exactly along the interface and this mode is decoupled, only $\text{Re}\{p\}=0$ modes will be used for comparison with the acoustical phonons obtained from the discrete calculations (Sec. III). The influence of the springlike interfacial conditions is investigated from dispersion, amplitude attenuation, and the polarization of the waves. In this problem the wave number k or wavelength $\lambda=1/k$, calculated as the eigenvalues of (9), not only depend on the velocity v for a given bicrystal but also on the interfacial properties $\hat{\mathbf{M}}^I$. Note that some of the characteristics of wave solutions are independent of interfacial conditions. For example, only behavior of $\text{Im}\{p\}$ as a function of v determines if such waves become bulklike in the long-wavelength limit, i.e., $\lambda\to\infty$ or $|k|\to 0$. The small wave number limit is achieved when v approaches either perfect bonding velocity $v_{\text{p.b.}}$ from left or from right or when $v\to(v_{\text{bulk}})_{\min}$. In this limit (9) reduces to $\det(\mathbf{H})=0$ which depends only on the bulk properties and the velocity of propagation.

First we consider continuum interfacial waves propagating along the tilt axis (x_2 or $\mathbf{\Gamma Y}$ direction) in the $\Sigma=5$ (120)/[001] grain boundary. Recall that "perfect bonding" Stoneley-type solutions [$h=0$ in (9), i.e., $\det\mathbf{H}=0$, which also corresponds to $k=0$] exist in this case at the calculated velocities $v/(v_{\text{bulk}})_{\min}=0.84$ in gold and 0.81 in copper.[9] (We find Stoneley solutions also exist for propagation directions lying in the interface within a ±5° range away from the tilt axis, but only for the wave propagating exactly along the tilt axis is $\text{Re}\{p\}=0$, otherwise the wave is "leaky.") The wavelength λ normalized by the lattice parameter a is plotted as a function of velocity in Figs. 8(a) and 8(b) for gold and copper, respectively, and for different choices of the thickness h of the interfacial layer in (9); note that $\hat{\mathbf{M}}^I$ which depends on h is determined without any adjustable parameters from the results of Ref. 12. There are two branches of solutions in the long-wavelength limit for these waves propagating along the tilt axis: one is for $v\to v_{\text{p.b.}}$ and the other for $v\to(v_{\text{bulk}})_{\min}$ and in both cases the velocity is nearly independent of wavelength, i.e., the solution is nearly nondispersive. This nondispersive character is exactly found for the Stoneley solutions which only exist at $v=v_{\text{p.b.}}$. The attenuation of these waves is plotted in Figs. 9(a) and 9(b); for these exponentially decaying wave solutions, i.e., $u\propto\exp(-|x_3|/\delta)$, where x_3 is the coordinate normal to the interface and $\delta=\lambda/\text{Im}\{p\}$. The attenuation becomes weaker, relative to the lattice dimension, as λ increases (or k decreases) which, from Fig. 8, occurs as $v\to v_{\text{p.b.}}$ and $v\to(v_{\text{bulk}})_{\min}$.

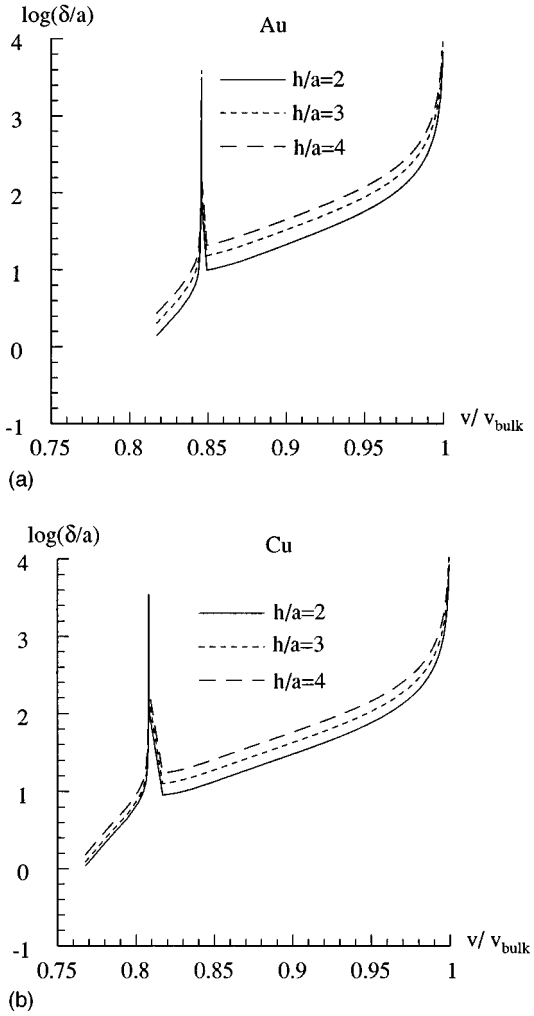

FIG. 9. Decay length δ (normalized by lattice parameter a) vs velocity v for subsonic interfacial waves propagating along the tilt axis ($\mathbf{\Gamma Y}$) (a) for B structure in gold and (b) for B' structure in copper ($\log=\log_{10}$).

The (elliptical) polarization of these waves, i.e., the direction of the displacement of material points, is defined from the products $\mathbf{A}^{(\alpha)}\cdot\mathbf{d}^{(\alpha)}$ in (5) and plotted in Figs. 10(a) and

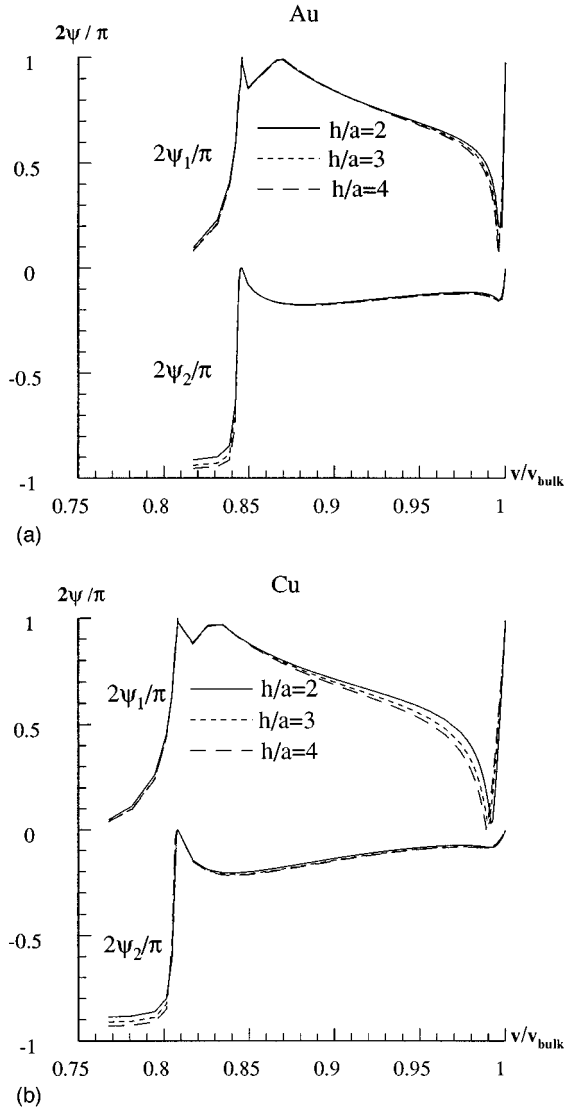

FIG. 10. Polarization plots (ψ_1, ψ_2 vs v) for subsonic interfacial waves propagating along the tilt axis (**ΓY**) (a) for B structure in gold and (b) for B' structure in copper.

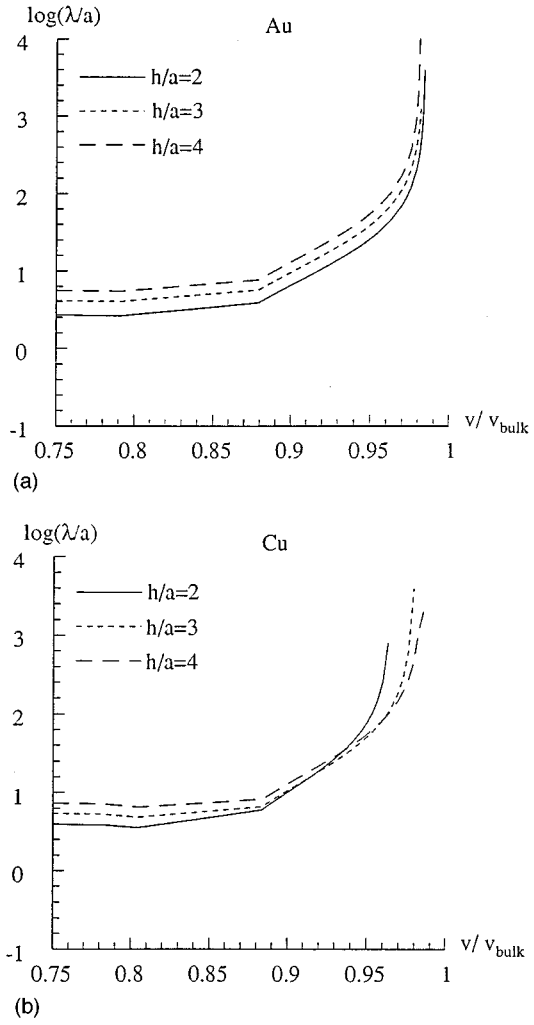

FIG. 11. Wavelength λ (normalized by lattice parameter a) vs velocity v for subsonic interfacial waves propagating perpendicular to the tilt axis (**ΓX**) (a) for B structure in gold and (b) for B' structure in copper (log=$\log_{10}$).

10(b) in terms of two angles ψ_1 and ψ_2 where for the wave propagation in the x_2 direction

$$\psi_1=\frac{2}{\pi}\tan^{-1}\left(\left|\frac{u_1}{u_3}\right|\right), \tag{10a}$$

$$\psi_2=\frac{-2}{\pi}\left|\cos^{-1}\left(\left|\frac{u_2}{|\mathbf{u}|}\right|\right)-\frac{\pi}{2}\right|. \tag{10b}$$

For $\psi_2=0$ the wave is purely transversal (shear); for $\psi_1=0$ with $\psi_2=0$ it is pure shear normal to the interface, and for $\psi_1=1$ with $\psi_2=0$ it is in-plane shear. For $\psi_2=-1$ (any ψ_1) the wave is purely longitudinal. The polarization depends on v (or λ) and can vary significantly from the perfect-bonding and bulk waves which, in the present case, are both dominated by in-plane shear for the direction of propagation parallel to the tilt axis. Therefore, the local properties of the interface region affect both the dispersion and attenuation of these interface waves.

Next we consider continuum interfacial waves propagating in the interface and perpendicular to the tilt axis (x_1 or **ΓX** direction) in the $\Sigma=5$ (120)/[001] grain boundary. Since the Stoneley-type solutions do not exist in this case,[9] the plots of wavelength versus velocity (Fig. 11) and decay-length versus velocity (Fig. 12) are simpler than for the case of waves propagating along the tilt axis. Again, these waves are dispersive with both wavelength and decay length increasing as the velocity increases up to $(v_{\text{bulk}})_{\text{min}}$. The polarization for these waves propagating in the x_1 direction are plotted in Fig. 13 in terms of the two angles

$$\psi_1=\frac{2}{\pi}\tan^{-1}\left(\left|\frac{u_2}{u_3}\right|\right), \tag{11a}$$

$$\psi_2=\frac{-2}{\pi}\left|\cos^{-1}\left(\left|\frac{u_1}{|\mathbf{u}|}\right|\right)-\frac{\pi}{2}\right| \tag{11b}$$

with the same interpretation of wave type with limiting values of ψ_1 and ψ_2 as in the preceding paragraph.

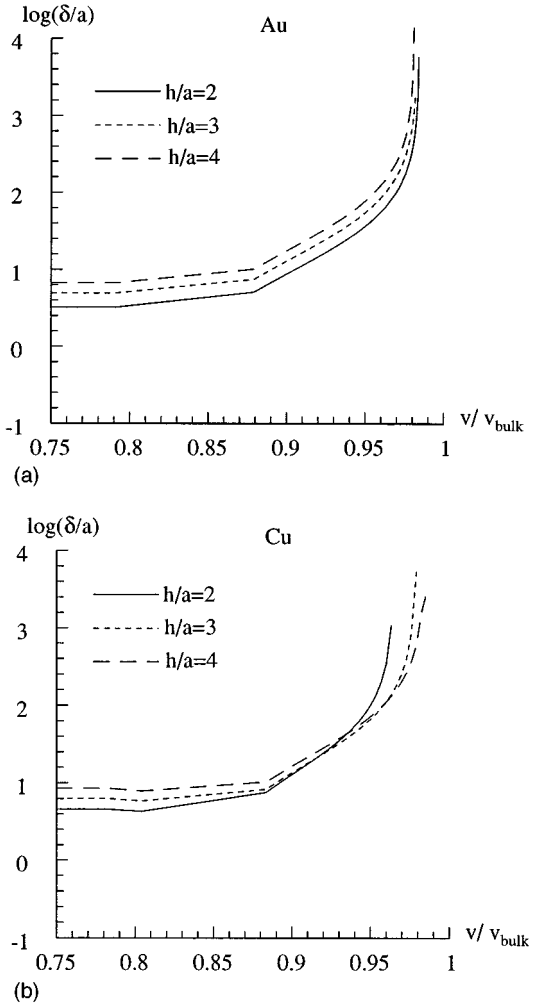

FIG. 12. Decay length δ (normalized by lattice parameter a) vs velocity v for subsonic interfacial waves propagating perpendicular to the tilt axis ($\mathbf{\Gamma X}$) (a) for B structure in gold and (b) for B' structure in copper.

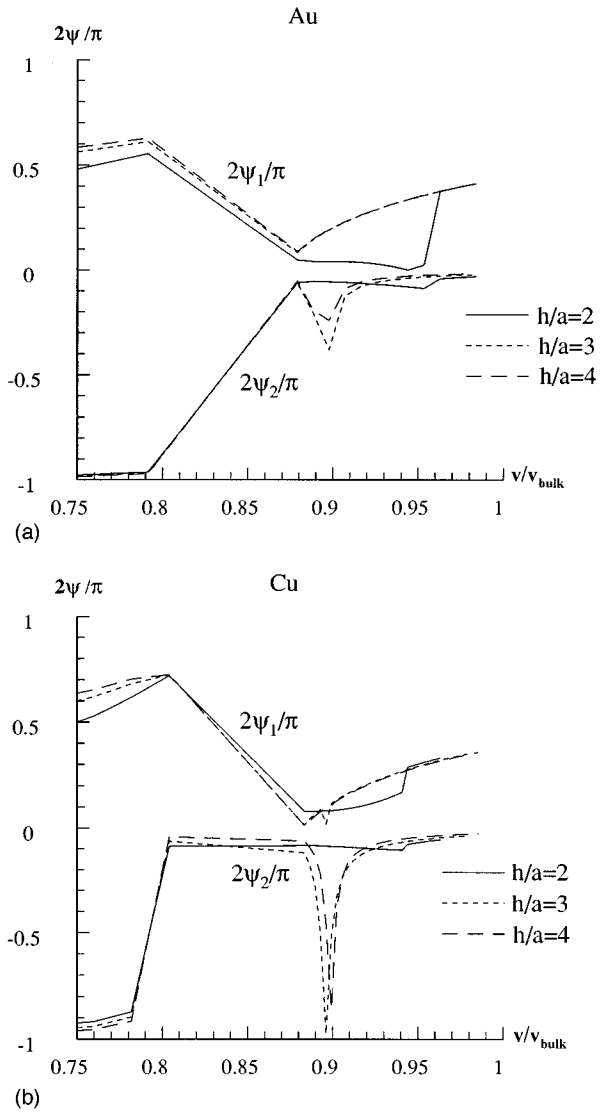

FIG. 13. Polarization plots (ψ_1,ψ_2 vs v) for subsonic interfacial waves propagating perpendicular to the tilt axis ($\mathbf{\Gamma X}$) (a) for B structure in gold and (b) for B' structure in copper ($\log=\log_{10}$).

V. COMPARISON BETWEEN CONTINUUM WAVES AND PHONONS

Phonons localized in the $\Sigma=5$ $(\overline{120})/[001]$ grain boundary and propagating perpendicular to and parallel to the tilt axis were calculated in Sec. III (parallel to the vectors $\mathbf{\Gamma X}=(1/5a)[210]$ and $\mathbf{\Gamma Y}=(3/10a)[002]$, respectively). The results plotted in Figs. 5–7 correspond to wavelengths $\lambda=44.7a$ and $\lambda=33.3a$ for the $\mathbf{\Gamma X}$ and $\mathbf{\Gamma Y}$ directions, respectively. The continuum solutions developed in Sec. IV will be compared at these wavelengths. These solutions also depend on the half-thickness h chosen to describe the interfacial region; note that h enters (9) explicitly and through $\hat{\mathbf{M}}^I(h)$, which is determined from (3) using the atomistic results.[12] Consistent with the trends in elastic moduli variations[12] [see Figs. 7(a) and 8(b) in that paper], particularly the extent of the grain-boundary region where the elastic properties differ from those of the ideal crystal being greater in gold than in copper, we have chosen $h/a=4$ for gold and $h/a=2$ for copper for the comparisons discussed below.

Table III gives the predicted continuum velocities (v_{cont}) from the solution to (9) as well as the calculated phonon velocities (v_{at}) at the same wavelengths, and it is seen that they are in reasonable agreement. Recall that the latter are for superlattices while the continuum solutions are for joined half-spaces. Also recall that ''perfect bonding'' Stoneley-type solutions [$h=0$ in (9), i.e., det$\mathbf{H}=0$, which also corresponds to $k=0$] exist only for waves propagating in the $\mathbf{\Gamma Y}$ direction at the velocities $v/(v_{\text{bulk}})_{\min}=0.84$ in gold and 0.81 in copper. The components of the polarization vector, i.e., the vector $\mathbf{A}^{(\alpha)}\cdot\mathbf{d}^{(\alpha)}$ in (5a) and (5c), are also listed in Table III and normalized so that the largest component has value of unity consistent with the phonon plots of Figs. 5–7. These components also compare favorably with the peaks of each component in those figures which are also listed in Table III. In particular, the wave propagating in the x_2 ($\mathbf{\Gamma Y}$) direction in gold is of the horizontal shear type, i.e., dominated by the x_1 component of displacement (as also predicted by the perfect bonding, Stoneley solution), while the corresponding wave in copper is of the vertical shear type, i.e., dominated by the x_3 component of displacement (which is inconsistent with the perfect bonding, Stoneley solution). Furthermore, the continuum solutions also satisfactorily reproduce trends in

TABLE III. Comparison of the continuum wave solutions with the subsonic phonon modes (see Table II).

Material/ wave vector	Wave-length	v_{at}/v_{bulk}	Phonon polarization (approx.)	v_{cont}/v_{bulk}	Continuum polarization
Au/**ΓX**	$44.7a$	0.96	[0.1,0,1]	0.95	[0.5,0.02,1]
Cu/**ΓX**	$44.7a$	0.97	[0.1,0,1]	0.96	[0.5,0.05,1]
Au/**ΓY**	$33.3a$	0.94	[1,0,0.1]	0.92	[1,0.17,0.27]
Cu/**ΓY**	$33.3a$	0.99	[0.01,0,1]	0.99	[0.3,0.13,1]

the decay length, where, as seen from Figs. 9(a) and 9(b), the decay length in copper tends to be longer than that in gold at the same wavelength.

The strong influence of the distinct interface structure and properties at these wavelengths that are considerably larger (at least an order of magnitude) than the thickness of the interfacial region has been demonstrated from detailed comparisons of the phonons with continuum models of elastic interface waves. The magnitude of the wavelengths (or smallness of wave number) considered were limited both from the separation of the grain boundaries in the superlattice and numerical considerations in the phonon calculations. Nevertheless, the continuum solutions for joined half-spaces can be interrogated at longer wavelengths where, from the results presented in Sec. IV, it is seen that the interface properties play an important role even at longer wavelengths. Nevertheless, in the long-wavelength limit, i.e., as $\lambda \to \infty$ or $k \to 0$, the continuum solutions are independent of interface properties as one would expect (except for extremes in properties, e.g., no resistance to shear) and yield one or possibly two velocities for this boundary: $v \to v_{\text{p.b.}}$ if the perfect bonding solution exists (for propagation in the **ΓY** direction) or $v \to v_{\text{bulk}}$ (in both the **ΓX** and **ΓY** directions) the effect of interface is lost and only bulk properties determine the form (polarization, attenuation, dispersion behavior) of the wave solutions.

In summary, we have seen that phonon spectra of bicrystals with relaxed grain-boundary structure display a variety of localized modes including long-wavelength acoustic modes. Continuum solutions for localized waves that incorporate atomic-level elastic properties of the interface via discontinuity relations agree well with the latter modes. In contrast, classical solutions that depend only on bulk elastic properties do not. This demonstrates that the distinct atomic structure of the interface is a controlling factor, and it is shown how local, atomic-level properties can be incorporated into continuum analyses of interfacial phenomena.

ACKNOWLEDGMENT

This research was supported by the National Science Foundation, Grant No. DMR94-12887. Research facilities were provided by the Laboratory for Research on Structure of Matter at the University of Pennsylvania supported by the NSF MRSEC Program DMR92-20668.

[1] J. S. Nelson, E. C. Sowa, and M. S. Daw, Phys. Rev. Lett. **61**, 1977 (1988).
[2] *Surface Phonons*, edited by W. Kress and F. W. DeWette, Springer Series in Surface Science Vol. 21 (Springer, New York, 1991).
[3] F. W. DeWette, in *Surface Phonons* (Ref. 2), p. 67.
[4] S. Aharon and A. Brokman, Acta Metall. Mater. **39**, 2489 (1991).
[5] R. Stoneley, Proc. R. Soc. London Ser. A **106**, 416 (1924).
[6] D. M. Barnett, J. Lothe, S. D. Gavazza, and M. J. P. Musgrave, Proc. R. Soc. London Ser. A **402**, 153 (1985).
[7] M. Cardona, Superlatt. Microstruct. **4**, 27 (1989).
[8] E. H. Elboudouti, B. Djafari-Rouhani, E. M. Khourdifi, and L. Dobrzynski, Phys. Rev. B **48**, 10 987 (1993).
[9] E. S. Alber, J. L. Bassani, V. V. Vitek, and G. J. Wang, Comp. Sim. Mater. Sci. Eng. **2**, 455 (1994).
[10] B. Djafari-Rouhani, P. Masri, and L. Dobrzynski, Phys. Rev. B **15**, 5690 (1977).
[11] B. Djafari-Rouhani, L. Dobrzynski, and P. Masri, Ann. Phys. (Paris) **6**, 259 (1981).
[12] I. Alber, J. L. Bassani, M. Khantha, V. Vitek, and G. J. Wang, Philos. Trans. R. Soc. London Ser. A **339**, 555 (1992).
[13] W. Bollman, *Crystal Defects and Crystalline Interfaces* (Springer, Berlin, 1970).
[14] A. P. Sutton and V. Vitek, Philos. Trans. R. Soc. London Ser. A **309**, 1 (1983).
[15] M. W. Finnis and J. E. Sinclair, Philos. Mag. A **50**, 45 (1984).
[16] G. J. Ackland, G. Tichy, V. Vitek, and M. W. Finnis, Philos. Mag. A **56**, 735 (1987).
[17] M. S. Daw and M. I. Baskes, Phys. Rev. B **29**, 6443 (1984).
[18] R. A. Johnson, Phys. Rev. B **37**, 3924 (1988).
[19] G. J. Ackland, M. W. Finnis, and V. Vitek, J. Phys. F **18**, L153 (1988).
[20] P. D. Bristowe and A. G. Crocker, Acta Metall. **25**, 201 (1977).
[21] G. J. Wang, A. P. Sutton, and V. Vitek, Acta Metall. **32**, 1093 (1984).
[22] G. J. Wang, V. Vitek, I. Alber, and J. L. Bassani, in *Materials Theory and Modeling*, edited by J. Broughton, P. Bristowe, and J. Newsam, MRS Symposia Proceedings No. 291 (Materials Research Society, Pittsburgh, 1993), p. 485.
[23] G. J. Wang, V. Vitek, I. Alber, J. L. Bassani, and G. Tichy, in *Intergranular and Interphase Boundaries in Materials: iib92*, edited by P. Komninou and A. Rocher, Materials Science Forum Vol. 126–128 (Trans Tech Publications, Aedermannsdorf, 1993), p. 337.
[24] R. E. Allen, G. P. Alldredge, and F. W. DeWette, Phys. Rev. B **4**, 1661 (1971).

[25] N. W. Ashcroft and N. D. Mermin, *Solid State Physics* (Saunders College, Philadelphia, 1976).
[26] W. Kress, in *Surface Phonons* (Ref. 2), p. 209.
[27] J. L. Bassani, V. Vitek, and I. Alber, Acta Metall. Mater. **40**, S307 (1992).
[28] J. L. Bassani and J. Qu, *Metal-Ceramic Interfaces*, Acta/Scripta Metallurgica Proceedings Series 4, edited by M. Rühle, A. G. Evans, M. F. Ashby, and J. P. Hirth (Pergamon, Oxford, 1990), p. 401.
[29] Z. Hashin, Mech. Mater. **8**, 333 (1990).
[30] Z. Suo, A. Needleman, and M. Ortiz, J. Mech. Phys. Solids **40**, 614 (1992).
[31] J. R. Willis, Adv. Appl. Mech. **21**, 1 (1981).
[32] E. S. Alber, Ph.D. dissertation, University of Pennsylvania, 1993.
[33] P. Chadwick and T. C. T. Ting, Q. Appl. Math. **45**, 419 (1987).
[34] W. Kahan, Proc. Am. Math. Soc. **41**, 11 (1975).
[35] E. S. Alber, J. L. Bassani, V. Vitek, and G. J. Wang, *Anisotropy, Inhomogeneity, and Nonlinearity in Solid Mechanics*, edited by D. F. Parker and A. H. England (Kluwer, Dordrecht, 1995), p. 437.